Contrib Mineral Petrol (2002) 142: 640–652
DOI 10.1007/s00410-001-0327-4

**E.B. Watson · D.A. Wark · J.D. Price**
**J.A. Van Orman**

# Mapping the thermal structure of solid-media pressure assemblies

Received: 3 July 2001 / Accepted: 24 September 2001 / Published online: 3 January 2002
© Springer-Verlag 2002

**Abstract** The refractory oxides MgO and $Al_2O_3$ are the most commonly used insulator/filler materials in solid-media pressure assemblies. These oxides react with one another at high temperatures and pressures, forming a well-defined layer of spinel ($\sim MgAl_2O_4$) at the contact. The spinel layer widens in proportion to the square root of time at a rate that also depends systematically upon temperature and pressure. On the basis of 44 piston-cylinder runs spanning 1,200–2,000 °C and 1.0–4.0 GPa, we present a general relationship describing the width ($\Delta X$) of the spinel layer as a function of time (t, in s), temperature (T, in K) and pressure (P, in GPa): $\Delta X = \left[8.58 \times 10^{11} \cdot \exp\left(-48865/T - 2.08 \cdot P^{1/2}\right) \cdot t\right]^{1/2}$. If the pressure and duration of an experiment are known (as is usually the case) this calibration makes it possible to calculate the temperature to within a few degrees at any location in a solid-media assembly where MgO and $Al_2O_3$ are in contact (at T above ~1,200 °C) – simply by measuring the width of the spinel layer with an optical microscope. Application of this "reaction-progress" thermometer to the 13- and 19-mm diameter piston-cylinder assemblies used in the RPI lab confirms generally parabolic axial T gradients with acceptably broad hot spots. Three-dimensional maps of the 19-mm assembly reveal a radial component to the thermal field, with somewhat higher temperatures near the graphite heating element (i.e., a saddle-shaped hot region). Two exploratory experiments in a multi-anvil apparatus at 14 GPa (1,700 and 1,975 °C) confirm that the reaction-progress technique will work at pressures well above 4 GPa. The piston-cylinder-based calibration predicts $\Delta X$ to within a factor of two in the two multi-anvil runs, and relative changes in T along the assembly can be readily mapped. However, additional high-pressure calibration points will be needed before the thermometer can be used in quantitative multi-anvil applications. The spinel reaction-progress thermometer is easily implemented, and should allow other researchers to map the thermal structures of their own assemblies in a single experiment with one thermocouple.

E.B. Watson (✉) · D.A. Wark · J.D. Price
Department of Earth and Environmental Sciences,
Rensselaer Polytechnic Instutute, Troy,
New York 12180-3590, USA
E-mail: watsoe@rpi.edu
Tel.: +1-518-2768838
Fax: +1-518-2766680

J.A. Van Orman
Carnegie Institution of Washington,
Geophysical Lab/DTM, 5251 Broad Branch Road,
NW, Washington, DC 20015-1305, USA

Editorial responsibility: T.L Grove

## Introduction

For several decades, solid-media devices have been the principal means of high-temperature experimentation at pressures exceeding 1 GPa. Among the various machines in widespread use today, the piston-cylinder apparatus (e.g., Boyd and England 1960) is the most commonplace, and is now a standard component of experimental geoscience laboratories worldwide. The piston-cylinder is routinely capable of pressures up to ~4 GPa and sustained temperatures approaching 2,000 °C, making it well-suited for studies spanning the range of P–T conditions in the lithosphere.

Beginning with the earliest piston-cylinder investigations, researchers have had to contend with a major limitation that applies to all solid-media devices – i.e., that temperature gradients within the pressure assembly place severe restrictions on sample size. Because the pressure medium is in direct contact with cold steel or carbide, large temperature gradients within the assembly are unavoidable. Accordingly, if the sample of interest is to be at a uniform temperature, it must be accommodated within the localized "hot spot" of the pressure assembly, which is generally near the midpoint of a tubular graphite heating element coaxial with the cylindrical assembly. Sample miniaturization has been the main strategy used to achieve uniform sample temperature.

To our knowledge, Kushiro (1976) was the first to take steps to alter the temperature distribution in a piston-cylinder assembly. Motivated by his need for a large, isothermal reservoir of molten rock in which to make high-pressure viscosity determinations, he tapered the walls of the tubular graphite heating element in order to vary the electrical resistance along its length. This innovation produced a significantly broader hot spot, confirmed by measurement of the temperature at three isolated points along the axis of the assembly.

A few researchers have actually taken advantage of the innate temperature gradients in piston-cylinder assemblies. Walker and coworkers characterized Soret diffusion in silicate melts (e.g., Walker et al. 1981; Lesher and Walker 1986), and melt migration in partially molten ultramafic rocks (e.g., Lesher and Walker 1988; Walker and Agee 1988). Watson and Wark (1997) used the temperature gradient to drive a flux of dissolved $SiO_2$ in quartz-saturated supercritical $H_2O$, a strategy that enabled extraction of solute diffusivities from the total mass of $SiO_2$ transported in a given time. Despite these few positive applications, the temperature gradient in solid-media pressure assemblies is more often a plague than a boon. It is a potential cause of deviations from chemical equilibrium, and can lead to microstructural pathologies such as textural elongation (e.g., Takahashi 1986; Walker and Agee 1988) and fluid channelization (Wark and Watson 2001).

Here we take the view that the temperature gradient in a high P–T device, whether detrimental or useful to a given investigation, must be well characterized in order to optimize the experimental results. We present a simple method for detailed mapping of the thermal structure of solid-media pressure assemblies. The method requires only a single thermocouple in the assembly. In most cases, the results can be assessed with an optical microscope, which provides a temperature resolution of a few degrees under optimal conditions. The technique offers the added advantage of recording the duration of prematurely quenched experiments, and may also be useful as an internal pressure monitor, or even as a means to investigate thermal properties of minerals and rocks at high pressures.

## General strategy and background

The common approach to measuring temperature in geological materials is to apply a calibrated thermometer based on the temperature-dependent partitioning of an element or elements between phases presumed to be in equilibrium. This approach might be successful in mapping temperature in solid-media pressure assemblies, but it would require special materials, lengthy and costly analytical procedures, and demonstrated attainment of equilibrium. We propose instead a "reaction progress" thermometer based upon the rate of reaction between the two refractory oxides most commonly used in solid-media pressure assemblies: MgO (periclase) and $Al_2O_3$ (corundum). These oxides are unstable together and react to form spinel (nominally $MgAl_2O_4$) over the range of conditions relevant to piston-cylinder experimentation. At a planar contact between MgO and $Al_2O_3$, the reaction produces a layer of spinel whose thickness is systematically dependent upon temperature, pressure, and time. The thickness of the spinel layer is readily characterized by optical microscopy in samples run at temperatures of ~1,200 °C or higher for reasonable durations (i.e., a few days at the low end of the temperature range). The goals of this paper are twofold: (1) to present a calibration of the rate of spinel growth as a function of temperature (and pressure); and (2) to apply the calibration to reveal the thermal structure of selected piston-cylinder and multi-anvil assemblies used at the Rensselaer Polytechnic Institute (RPI) and the Geophysical Lab, respectively. The calibration is based exclusively upon 44 piston-cylinder runs made at RPI (1–4 GPa). However, two additional experiments were run in a multi-anvil apparatus at the Geophysical Lab to explore the potential of implementing the "reaction-progress" method at higher pressures.

As a summary of spinel growth-rate measurements, this paper has many precedents. The importance of MgO and $Al_2O_3$ in refractory ceramics has stimulated investigations by materials scientists for four decades, and numerous papers have been published in which 1-atm spinel growth-rate data are reported and the reaction mechanism deduced and debated (see, e.g., Carter 1961; Rossi and Fulrath 1963; Yamaguchi and Tokuda 1967; Whitney and Stubican 1971a, 1971b; MacKenzie and Ryan 1981; Li et al. 1992; Zhang et al. 1996; Ting and Lu 1999). The results reported here extend the existing data base to high pressures, and also constitute an internally-consistent set of data covering a wider range of temperature (1,200–2,000 °C) than any single previous study. We have our own model of the diffusion-controlled reaction, which is described in detail in a companion paper (Watson and Price 2001).

## Materials, conditions, and methods

### Materials

The idea of developing a reaction-progress thermometer for piston-cylinder work grew out of the simple observation that the $Al_2O_3$ thermocouple insulator in our assemblies reacts with the surrounding polycrystalline MgO to form a well-defined spinel layer of locally uniform thickness (Fig. 1). As discussed below, our growth-rate calibration was obtained simply by measuring the thickness of spinel layers formed between contacting MgO and $Al_2O_3$ filler pieces of our assemblies. The rationale for using standard assembly parts was simply that, in order for our thermometer to be useful to us and to others, it should be based upon the ordinary materials used in everyday experimentation

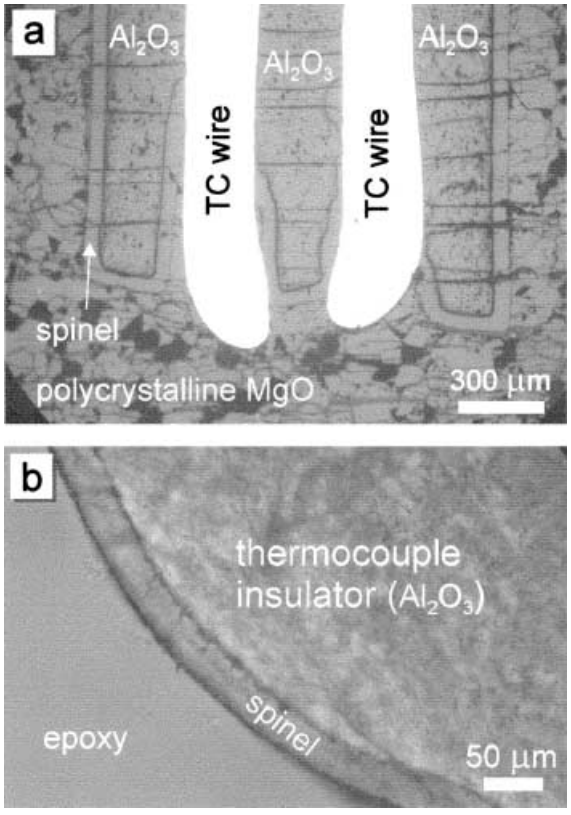


**Fig. 1** **a** Reflected-light photomicrograph of the region surrounding the thermocouple tip in run no. 9. The axis of the assembly lies vertically in the plane of the image. **b** Transmitted-light photomicrograph of the spinel rim on the $Al_2O_3$ thermocouple insulator, sectioned perpendicular to the assembly axis above the thermocouple tip of run 41. Epoxy replaces polycrystalline MgO that spalled away during sample preparation

(i.e., not upon high-purity oxides or single crystals). The thermocouple insulators and other dense alumina parts used in the piston-cylinder assemblies are purchased from Vesuvius McDanel and have a nominal purity of 99.8% $Al_2O_3$. The MgO filler pieces are supplied by Saint-Gobain/Norton as 99.7% MgO machinable ceramic ($SiO_2$ and $Al_2O_3$ are the main impurities reported by the supplier). Most of the spinel-thickness measurements were taken from the interface between the thermocouple insulator and contacting MgO, although several other arrangements of the standard MgO and $Al_2O_3$ components were also used (see Fig. 2). The more complex assemblies were designed to assess possible geometric effects (e.g., curved vs. flat interfaces) as well as axial and radial variation of spinel thickness within the assembly. To supplement the data obtained from reaction between polycrystalline MgO and $Al_2O_3$, we performed several piston-cylinder experiments using high-purity single crystals of periclase and corundum arranged as "sandwiches" (see Watson and Price 2001). These experiments were designed to shed light on the inter-diffusion processes involved in spinel growth, and so are not discussed in detail here. Significantly, however, the single-crystal data are generally indistinguishable from those for the ordinary polycrystalline materials. This result is encouraging for two reasons: it rules out possible reactant grain-size effects on spinel growth, and it suggests that the growth rate is not critically dependent upon impurity levels of the reacting oxides (this suggests, further, that our spinel-growth systematics are transferable to MgO and $Al_2O_3$ filler pieces supplied by other manufacturers).

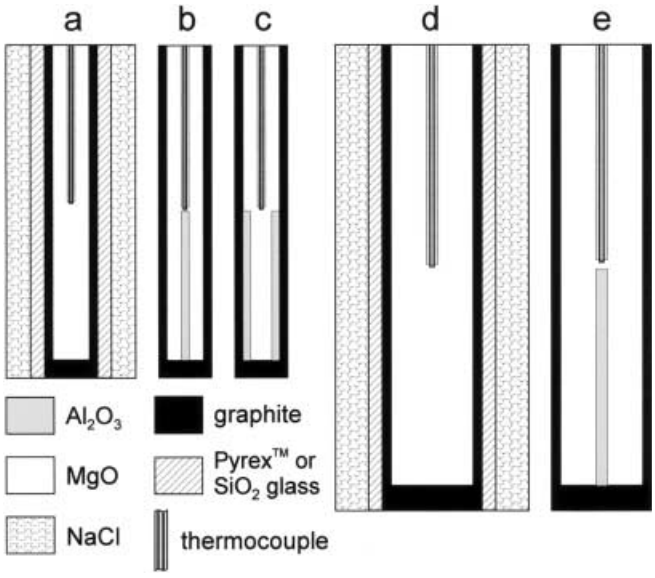


**Fig. 2a–e** Scale drawings representing axial sections through the piston-cylinder assemblies used in this study. Sketches **a**–**c** portray the smaller, 13-mm diameter assemblies (NaCl sleeve omitted from **b** and **c**). Sketches **d** and **e** show two of the 19-mm diameter assemblies (NaCl sleeve omitted from **e**; see also Fig. 7)

The materials reacting to form spinel in the two multi-anvil runs were dense, polycrystalline $Al_2O_3$ supplied by Alfa Aesar (99.7% nominal purity), and either high-purity (99.998%) MgO powder from Alfa Aesar (run MA1) or polycrystalline MgO rod (99.75% nominal purity) from Norton Company (run MA3).

## Piston-cylinder experiments

The piston-cylinder experiments were conducted in an end-loaded, Boyd and England (1960) type apparatus, using 13- and 19-mm-diameter pressure assemblies consisting of an NaCl outer sleeve, a glass thermal insulator sleeve (Pyrex or $SiO_2$, depending upon the P–T conditions of the individual experiment), and a tubular graphite heater (see Fig. 2). As noted previously, several different arrangements of the MgO and $Al_2O_3$ filler pieces inside the heater were used. In all cases, the ceramic pieces were pre-dried at 700 °C for at least 2 h immediately prior to running an experiment. The experimental conditions range from 1,200 to ~2,000 °C and 1.0 to 4.0 GPa, although only a few runs were made at pressures above 3.2 GPa and temperatures above 1,700 °C. Below 1,200 °C, the rate of spinel formation was too slow to measure accurately by conventional means in experiments of reasonable duration. Table 1 summarizes the conditions and durations of all experiments from which usable data were obtained.

A single $W_{97}Re_3/W_{75}Re_{25}$ thermocouple was used in all piston-cylinder experiments, with no correction for the recognized pressure effect on the emf (Mao and Bell 1971). A change in thermocouple wire lots was made after run number 51; this is noteworthy because the calibration of the new wire spools was significantly different from that used in the vast majority of runs, especially at temperatures in excess of ~1,500 °C. A correction was therefore applied to the nominal temperatures of some runs made late in the study (nos. 52–54) in order to make them consistent with the rest of the experiments (this is the why the temperatures of these runs depart from the normal 100-degree interval; see Table 1). The sample pressure was taken as that given directly by the oil pressure acting on the hydraulic ram driving the carbide piston. Previous calibrations in our laboratory based on the melting curves of Au and NaCl have shown that our cell design is essentially "friction-

less" in the 1.0–1.5-GPa range, with apparent pressures within ~20 MPa of actual values. The experiment run-up involved cold pressurization to a value exceeding the desired run pressure by 10–20%, allowing for "settling" (relaxation) of the assembly upon heating. The final desired run pressure is closely approached using this technique, necessitating only minor (upward) pressure adjustments later in the run in most cases. This run-up procedure could be described as "hot piston-in"; however, such a characterization is probably too simplistic because runs of extended duration require repeated minor upward adjustments in apparent pressure over the first ~2–~24 h, depending upon temperature.

Experiments were terminated by thermal quenching (~10 s for 13-mm assemblies; 20–30 s for 19-mm assemblies) followed by depressurization and recovery of the assembly from the pressure vessel. The NaCl pressure medium and the glass insulator sleeve were removed and the remaining parts of the cell impregnated with epoxy to limit disaggregation along decompression cracks (not always completely successful). The assembly was then sawn in two close to the cylinder axis. The larger piece was impregnated a second time and cast in epoxy, then ground with a diamond whetstone to expose an axial section. The ground surface was prepared for spinel thickness measurements by polishing with 1-μm alumina followed by colloidal silica.

**Table 1** Summary of run information and spinel layer thicknesses

| Experiment no. | T (°C) | P (GPa) | Size[a] | Duration (h) | $\Delta X_m$ (μm) |
|---|---|---|---|---|---|
| 9 | 1,600 | 2.5 | S | 4.5 | 50 |
| 10 | 1,400 | 2.5 | S | 88.1 | 48 |
| 11 | 1,300 | 2.5 | S | 118.1 | 20 |
| 12 | 1,600 | 2.5 | S | 21.0 | 97 |
| 13 | 1,600 | 2.5 | S | 1.0 | 26 |
| 14 | 1,600 | 2.5 | S | 10.0 | 70 |
| 15 | 1,600 | 2.5 | S | 2.0 | 35 |
| 16 | 1,200 | 2.5 | S | 167.3 | 8 |
| 17 | 1,500 | 2.5 | S | 20.0 | 60 |
| 18 | 1,700 | 2.5 | S | 1.5 | 60 |
| 19 | 1,700 | 2.5 | S | 15.7 | 175 |
| 20 | 1,700 | 2.5 | S | 6.0 | 105 |
| 21[b] | 1,500 | 2.5 | S | 64.3 | 93 |
| 22 | 1,500 | 2.5 | S | 5.7 | 30 |
| 23 | 1,400 | 1.0 | L | 48.0 | 62 |
| 25[b] | 1,600 | 2.5 | S | 48.0 | 152 |
| 26 | 1,500 | 2.5 | S | 1.5 | 13 |
| 27[b] | 1,400 | 2.5 | S | 24.0 | 24 |
| 28 | 1,300 | 2.5 | S | 64.7 | 12 |
| 29 | 1,700 | 2.5 | S | 0.4 | 28 |
| 30 | 1,400 | 2.5 | S | 4.0 | 13 |
| 31 | 1,300 | 2.5 | S | 16.0 | 8 |
| 32 | 1,400 | 1.7 | S | 48.0 | 50 |
| 33 | 1,400 | 1.7 | S | 16.0 | 27 |
| 34 | 1,600 | 1.7 | S | 2.0 | 46 |
| 35 | 1,400 | 3.2 | S | 64.0 | 32 |
| 36 | 1,600 | 3.2 | S | 2.0 | 29 |
| 37 | 1,600 | 1.0 | S | 0.05 | 9 |
| 38 | 1,400 | 3.2 | S | 18.0 | 18 |
| 39 | 1,600 | 3.2 | S | 16.0 | 66 |
| 40 | 1,600 | 1.7 | S | 12.0 | 103 |
| 41 | 1,400 | 1.0 | L | 20.0 | 40 |
| 42 | 1,600 | 1.0 | L | 2.0 | 65 |
| 44 | 1,200 | 3.2 | S | 240.0 | 8 |
| 46 | 1,200 | 1.7 | S | 240.0 | 12.5 |
| 47[b] | 1,400 | 1.7 | L | 30.0 | 35 |
| 48 | 1,400 | 1.7 | L | 72.0 | 50 |
| 49 | 1,200 | 4.0 | S | 191.8 | 6 |
| 50 | 1,400 | 4.0 | S | 89.4 | 30 |
| 51 | 1,500 | 1.7 | L | 23.5 | 74 |
| 52 | 1,780 | 2.5 | S | 1.0 | 65 |
| 53 | 1,879 | 2.5 | S | 1.0 | 118 |
| 54 | 1,978 | 2.5 | S | 0.4 | 115 |
| 56[b] | 1,400 | 1.7 | L | 23.3 | 32 |
| MA1 | 1,700 | 14.0 | n.a. | 13.9 | 9 |
| MA3 | 1,975[c] | 14.0 | n.a. | 2.3 | 14 |

[a] Size of piston-cylinder assembly: *S* 13-mm diameter; *L* 19-mm diameter

[b] Thermally mapped assemblies

[c] Temperature estimated on the basis of furnace power consumption (see text)

## Multi-anvil experiments

The two exploratory multi-anvil experiments were performed in a Walker-style multi-anvil apparatus at the Geophysical Laboratory, Carnegie Institution of Washington (Bertka and Fei 1997) using 25.4-mm Toshiba F-grade tungsten carbide anvils with 3-mm triangular truncations. The anvils were separated by compressible pyrophyllite gaskets. The octahedral assembly (8-mm edge length) was pre-cast MgO doped with $Cr_2O_3$. A cylindrical hole was drilled in the pressure medium for the insertion of a 1-mm-thick $LaCrO_3$ insulating sleeve, which surrounded a straight-walled Re heating element 0.064 mm thick. The MgO rod or powder reacting to form spinel was contained in a sleeve of dense $Al_2O_3$ 1.0 mm I.D.×1.5 mm O.D. This sleeve was centered in the furnace using two alumina end caps. The temperature was monitored during the experiment with a W5%Re–W26%Re thermocouple inserted axially into the assembly through holes in one of the alumina end caps.

## Spinel thickness measurements

As noted previously, most spinel-thickness measurements were made at the contact between the polycrystalline $Al_2O_3$ thermocouple insulator and the surrounding MgO. The insulator surface is cylindrical, so care was needed to ensure the true thickness of the spinel was obtained from the planar section. This was straightforward in the crucial region near the thermocouple tip (i.e., where the temperature is known) because the sample sections can be ground to just expose the junction of the thermocouple wires. At this location, the thickness of the spinel layer on the end of the thermocouple insulator can be compared with the thickness on the cylindrical surface (see Fig. 1). In cases where spinel thickness measurements were desired along the length of the thermocouple insulator (or along the alumina capsule wall in the case of the multi-anvil runs), the task was more challenging because of slight but inevitable deformation of the assembly parts.

Three different methods were evaluated for suitability in gauging the thickness of the spinel layer. In order of increasing complexity, these were (1) visual estimates made with a 15× micrometer ocular on a reflected-light optical microscope (20× objective); (2) digital estimates from back-scattered-electron (BSE) images obtained with an electron microprobe (EMP); and (3) digital estimates from X-ray raster maps, also obtained with the EMP. The three techniques were found to give consistent results, so the simple, inexpensive optical microscope was adopted for the measurements that form the basis of our growth-rate calibration (i.e., all those reported in Table 1 for piston-cylinder runs). Spinel layer thicknesses in the multi-anvil run products were determined from 80×80-μm digital element maps made with the electron microprobe. The thicknesses of layers formed at curved and planar $MgO/Al_2O_3$ contacts in the same sample were found to be indistinguishable, thus eliminating concern about possible radial effects on spinel growth in the cylindrical geometry (the lack of a detectable 3-D geometric effect is because of the large radius of curvature of the $MgO/Al_2O_3$ contact relative to the thickness of the spinel layer). The spinel thicknesses reported in Table 1 for piston-cylinder runs were all obtained within 0.5 mm of the thermocouple, i.e., within the "hot spot" of the assembly. The uncertainties in these values, based upon variability among three to six visual measurements

using the micrometer ocular, are estimated at ±2–3 μm in the worst case. This estimate should be regarded as the reproducibility if the measurements within a given region of the assembly; it does not take into account inaccuracies that might conceivably arise from "sectioning errors" (i.e., fortuitous intersections of the polished surface with a periclase/corundum contact that is steeply dipping because of undetected deformation).

Because of the difference in the technique used to gauge spinel thickness in the multi-anvil runs, the uncertainty estimates are also reported in a different way (and appear as error bars in the relevant plots). In this case, digital determinations of spinel thickness were made at 5-μm intervals on the 80 × 80-μm element maps. Several contiguous measurements (usually eight to ten) were then bundled together and a mean and standard deviation recorded for each bundle along with a midpoint coordinate.

## Spinel growth-rate calibration to 4 GPa

Figure 3 summarizes data on spinel growth between contacting polycrystalline MgO and $Al_2O_3$ for 43 experiments listed in Table 1. The thickness of the spinel layer ($\Delta X$) is plotted against the square root of time in the expectation of a linear relation signifying diffusion control (see Watson and Price 2001). Following Tammann (1920), it is customary and useful to convert reaction-product thicknesses from experiments such as ours to a reaction rate constant, $k = \Delta X^2/2t$, having the units of diffusivity. This was done by Watson and Price (2001) to produce a set of $k$ values that show a clear log-linear dependence on $T(K)^{-1}$ at constant pressure and a log-linear dependence on pressure at constant temperature (see Figs. 5 and 6 of Watson and Price 2001). These figures are not reproduced here in order to conserve space, and also because it is $\Delta X$, and not $k$, that is actually measured. Equations are provided below that allow computation of temperature directly from $\Delta X$. Watson and Price show, moreover, that $k$ is not a "pure" kinetic parameter, but rather a composite of kinetics (Mg↔Al inter-diffusion in spinel) and thermodynamic driving potential related to the composition of spinel coexisting with corundum (which depends upon both temperature and pressure). Even though $k$ is not a fundamental quantity, the highly systematic dependence of $\Delta X$ upon temperature and pressure can be used to great advantage in the practical application of mapping temperature in solid media pressure assemblies.

We attempted several regression strategies in our search for a general relationship describing the dependence of $\Delta X$ upon temperature (T), pressure (P), and time (t). All of these began with the assumption that $\Delta X \alpha t^{1/2}$, which is expected for diffusion-controlled growth of a reaction product, and which is convincingly borne out by the data (Fig. 3). If the variation in spinel growth rate with T and P were solely caused by the effects of these variables on the rate-controlling diffusivity, then it would make sense to regress $\ln k$ against $T(K)^{-1}$ and $P/T$, because the diffusion coefficient is generally proportional to $\exp[-(E_a + PV_a)/RT]$, where $E_a$ and $V_a$ are the activation energy and activation volume, respectively. This approach yields a reasonable result. As noted above, however, the rate of spinel growth is not determined solely by the governing diffusivity, so we were free to explore other empirical dependencies (as are motivated readers, because all the necessary data are included in Table 1). We present the results of two approaches, the first of which involved treating isobaric sets of data independently and fitting each set to an equation of the form:

$$\Delta X_c = [A \cdot \exp(-B/T) \cdot t]^{1/2} \quad (1)$$

where "A" and "B" are constants, $T$ is absolute temperature, $t$ is time in seconds and $\Delta X_c$ is expressed in microns. The results are shown in Fig. 4a as a plot of spinel thickness calculated using theÂequations ($\Delta X_c$) against the thickness actually measured on the samples ($\Delta X_m$) for isobars of 1.0, 1.7, 2.5, 3.2, and 4.0 GPa. The constants A and B for each isobar are given on the figure. Overall, this simple approach yields the lowest residuals of the various simple fitting strategies we tried.

The isobaric, single-regression equations shown in Fig. 4a have the obvious drawback that interpolation is required for estimating the extent of spinel growth at pressures other than those calibrated. Accordingly, we present an alternative "global" multiple-regression relation from which $\Delta X$ can be calculated for any pressure within the calibration range:

$$\Delta X_c = \left[8.58 \times 10^{11} \exp\left(-48865/T - 2.08 \cdot P^{1/2}\right) \cdot t\right]^{1/2} \quad (2)$$

where $P$ is expressed in GPa and $\Delta X_c$ again in microns. The results are shown in Fig. 4b as a comparison of measured vs. calculated $\Delta X$. The residuals for this approach are slightly higher than when the data are treated as independent isobars, but the correspondence between $\Delta X_c$ and $\Delta X_m$ is nevertheless quite good. For reasons discussed above, the $P^{1/2}$ term is strictly empirical and has no mechanistic significance of which we are aware. It was used in the regression analysis because we noted that $\ln(\Delta X^2/2t)$ depends linearly on $-P^{1/2}$ at temperatures near the middle of the range investigated. The choice of $P^{1/2}$ gives a slightly better result than does $P$ or $P/T$ in characterizing the overall pressure dependence of spinel growth in the piston-cylinder range.

It should be emphasized that the calibration embodied in Eq. (2) is not intended for quantitative use at pressures significantly above 4 GPa – that is, in multi-anvil experimentation. Interestingly, however, the piston-cylinder results can be used to roughly "predict" spinel thicknesses even at 14 GPa (see the Mapping section below). At this pressure, Eq. (2) overestimates $\Delta X$ by a factor of two. If, on the other hand, $\ln(\Delta X^2/2t)$ is assumed to depend upon $P/T$ (rather than $P^{1/2}$; see above) in the multivariate analysis of the piston-cylinder data, the resulting calibration underestimates the rate of spinel growth at 14 GPa by a factor of ~2. Clearly, many more high-pressure calibration points are needed for quantitative application of the reaction progress thermometer at multi-anvil pressures (see Van Westrenen et al. 2001).

A few calculations with Eq. (2) reveal that the rate of spinel growth is quite sensitive to changes in temperature and pressure under some circumstances. The equation is readily differentiated with respect to T or P, but the resulting expressions are cumbersome and provide little intuitive feeling for the sensitivity of $\Delta X$ to variations in T and P. The potential usefulness of our results can be appreciated from Fig. 5, which shows the extent of spinel growth in a 1-day experiment under various conditions (recall that $\Delta X$ scales with $t^{1/2}$, so all results would be doubled in a 4-day experiment). Figure 5a is a plot of $\Delta X$ as a function of temperature for isobars at 1, 2, and 3 GPa. Low temperatures and high pressures inhibit spinel growth, and at 1,200 °C and 3 GPa $\Delta X$ is only ~3 μm. At 1,600 °C and 1 GPa, in contrast, $\Delta X$ ~200 μm. The sensitivity of $\Delta X$ to changes in temperature at various conditions is conveyed by the temperature derivatives marked on the curves: over the range of conditions investigated, $\partial \Delta X/\partial T$ ranges from $< 0.05$ μm/°C (at low T and high P) to $> 2$ μm/°C (at high T and low P). Figure 5b is an analogous plot of $\Delta X$ as a function of pressure for isotherms at 1,200, 1,400, and 1,600 °C. The pressure derivatives shown on the figure range from ~0.7 μm/GPa to ~70 μm/GPa.

The $\partial \Delta X/\partial T$ and $\partial \Delta X/\partial P$ values should be considered in the context of how well $\Delta X$ can be measured on an actual run product. The resolution and reproducibility of $\Delta X$ measurements depends on the method used and the nature of the periclase/corundum couples. In principle, the higher magnification of an SEM- or EMP-based approach should yield a more accurate result. However, when the MgO and $Al_2O_3$ reactants are polycrystalline, the phase boundaries are slightly wavy (see Fig. 6a), so high magnification is not necessarily advantageous. Use of single-crystal reactant phases produces knife-edge phase boundaries (Fig. 6b, c) that allow measurement of $\Delta X$ with ~1-μm reproducibility even with an optical microscope. The drawback of single crystals, of course, is that they are not routine components of solid-media assemblies. Users of our thermo(baro)meter will no doubt adopt approaches that suit their

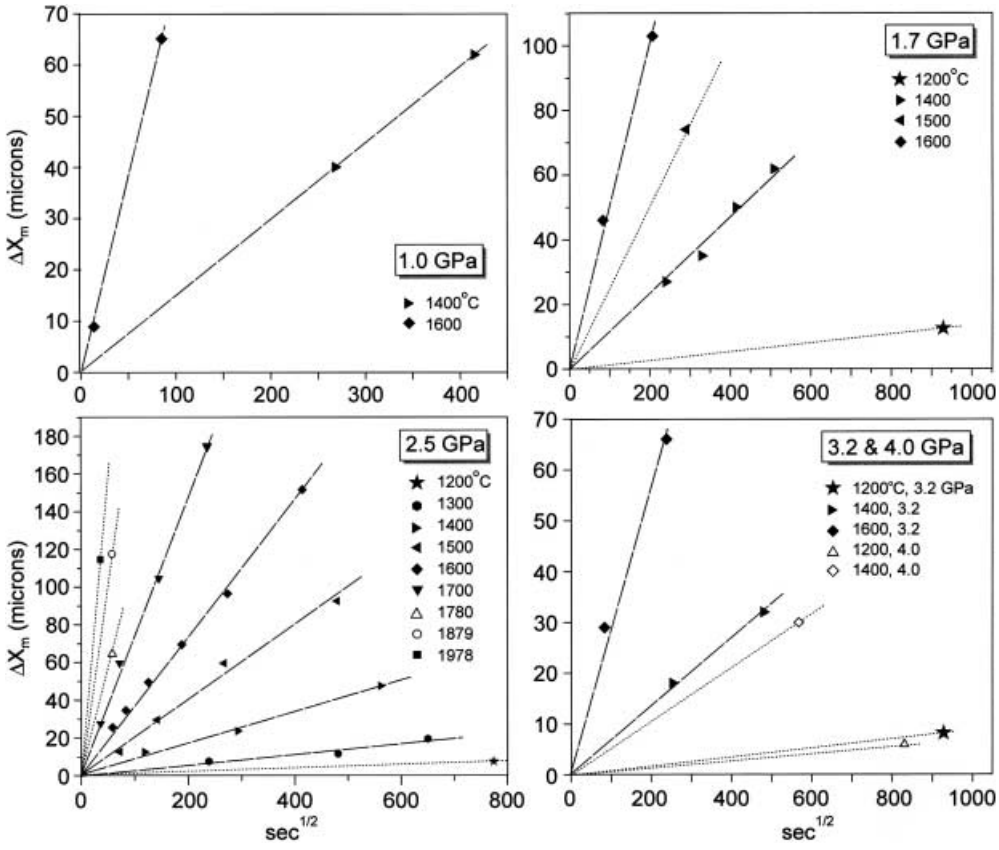


**Fig. 3** Measured spinel layer thickness ($\Delta X_m$) vs. the square root of run duration for experiments at 1.0, 1.7, 2.5, 3.2, and 4.0 GPa. The linear regressions (*dashed lines*) are constrained to pass through the origin; *dotted lines* are based on a single experiment

specific goals and needs. Most routine applications will probably involve characterization of thermal gradients in solid-media assemblies, where only relative measurements (i.e., spatial variation of $\Delta X$) will be needed. In this case, the quality of the result will probably depend more upon the statistical base (i.e., number of $\Delta X$ values measured) rather than the accuracy of any single measurement.

## Mapping (and controlling) temperature distribution

In this last section we illustrate the use of our spinel reaction-progress thermometer to map temperature distribution in solid-media pressure assemblies. The treatment is not exhaustive in that thermal structures are reported for only three piston-cylinder assembly designs at three temperatures and one multi-anvil design at two temperatures. This conservative approach is taken because other labs. use assembly components and dimensions that differ substantially from ours, so the transferability of detailed information will be limited. The procedure is simple enough that interested readers can easily map their own assemblies.

It can be appreciated from Fig. 2 that the extent of $MgO/Al_2O_3$ interface in some of the piston-cylinder assemblies used for the calibration runs is sufficient to allow assessment of both axial and radial temperature gradients. For the 13-mm assemblies, versions "b" and "c" together are adequate to characterize the axial thermal profile and demonstrate the absence of a detectable radial gradient (see below). A more complicated filler-piece geometry was required to capture the overall temperature distribution in the large-volume (19-mm) assembly, as shown in Fig. 7. Assemblies "a" and "b" in this figure have coaxial sleeves of MgO and $Al_2O_3$ outside the thermocouple insulator, which provide axis-parallel temperature monitoring at three radial distances from the assembly axis. These two assemblies differ only in the respect that "b" (run 56) includes a graphite insert to thicken the wall of the heater by ~0.5 mm near the mid-section of the assembly. This feature was added in an attempt to duplicate, in a cost-effective way, the broadening of the axial temperature profile that Kushiro (1976) achieved by tapering his graphite heater.

The configuration of the multi-anvil assembly used for thermal mapping is shown in Fig. 8 as a section that includes the thermocouple and the axis of the dense $Al_2O_3$ sleeve. Apart from overall size, a fundamental difference from the piston-cylinder assemblies in this application is that the thermocouple monitors temperature at one end of the sample region rather than at the hotspot.

Figure 9 shows axial temperature profiles for our 13-mm assembly (configuration "b" in Fig. 2) run at 2.5 GPa and three different thermocouple temperatures – 1,400, 1,500, and 1,600 °C (runs 21, 25, and 27 in Table 1). The profiles span the central portions of the assembly axes, i.e., a total of ~13 to ~17 mm vertical

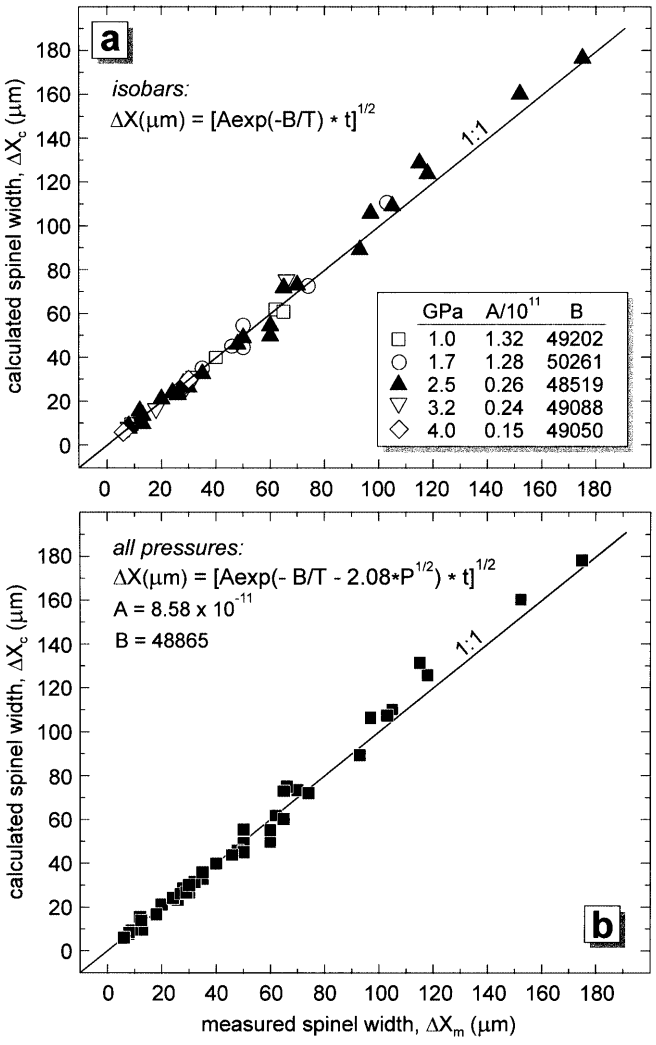


**Fig. 4a, b** Calculated spinel thicknesses ($\Delta X_c$) from Eqs. (1) and (2) plotted against actual measurements ($\Delta X_m$). In **a**, the calculated values come from Eq. (1), in which the constants have different values at isobars of 1.0, 1.7, 2.5, 3.2, and 4.0 GPa (*see inset*). In **b**, the $\Delta X_c$ values were computed using the "global" fit Eq. (2). See text for discussion

distance, depending upon the midpoint temperature. Readers should bear in mind that the overall height of the 13-mm diameter assembly is ~28 mm (including the graphite bottom-piece), compacted during the experiment from the initial assembly height of 32 mm. The temperature–distance profiles seem to be well represented by parabolas, with the possible exception of the 1,600° run, in which the "hot spot" appears somewhat flatter than the parabolic fit. However, there is obvious "noise" in the temperature data because of uncertainties in the $\Delta X$ measurements. Given the inevitable smoothing effects of heat conduction, the parabolas on the figure are probably reasonable representations of the thermal profiles actually present in the assemblies at run conditions (although there is no theoretical basis for expecting a strictly parabolic axial temperature distribution). As expected, the profiles narrow with increasing midpoint temperature to produce steeper gradients outside the hot zone. On the whole, however, the results should be reassuring to researchers doing phase-equilibrium studies because, even at these relatively high temperatures, there exists a central zone ~4 mm long in which the temperature variation is only ~20–25° even when the midpoint is at 1,600 °C (the variation drops to only 10–15° at a midpoint temperature of 1,400 °C). The temperature variation along a 2-mm sample is probably no more than ~5°, which is tolerable in most applications (but see Wark and Watson 2001).

Assembly design "c" in Fig. 2 has a periclase/spinel contact surface perpendicular to the assembly axis near its midpoint, and so can be used to assess radial temperature variation in the 13-mm assembly. We were unable to detect systematic changes in spinel thickness at this surface, or between the spinel layer at this surface and that formed between the thermocouple insulator and the surrounding MgO. If there is a radial gradient in the 13-mm assembly, it is too small to detect using polycrystalline reactants with the reaction-progress thermometer.

The larger volume of our 19-mm assemblies necessitated a more ambitious thermal mapping effort using the extensive periclase/spinel contact surface in the assemblies depicted in Fig. 7. The results for a standard assembly with a straight graphite heating element (run 47; 1,400 °C, 1.7 GPa) are shown in Fig. 10. The figure includes six axis-parallel temperature profiles in addition to a temperature contour map of the assembly and a three-dimensional contour plot. The contour map is superimposed on a tracing of the features exposed in the polished surface, and shows the precise location of the thermocouple and the contacts between MgO and $Al_2O_3$ where spinel thickness measurements were made. The obvious irregularities in the $MgO/Al_2O_3$ contact are caused by compression faults in the dense $Al_2O_3$, which develop because the surrounding MgO is not fully dense and weaker than the $Al_2O_3$. The salient aspects of the thermal structure are (1) the axial profile is significantly broader than is typical of the 13-mm diameter assemblies, which is expected given the ~12-mm difference in height (the post-experiment height of our 19-mm diameter assemblies is ~40 mm, compacted from an initial height of ~45 mm); (2) a hot spot characterized by a ~20° temperature variation spans ~7 mm along the axis; and (3) there is an unequivocal radial component to the temperature field characterized by 15–25° higher temperatures near the furnace wall along most of its length. The three-dimensional structure of the temperature field in the region of the thermocouple is saddle-shaped (see Fig. 10), in agreement with predictions based on finite-difference modeling (Wunder and Schilling 1999).

The results of our attempt to broaden the hot zone of the 19-mm assembly are shown in Fig. 11. This figure shows the thermal structure of run no. 56 (1,400 °C, 1.7 GPa), which was essentially a duplicate of no. 47 incorporating a "step-waisted" furnace (see above and

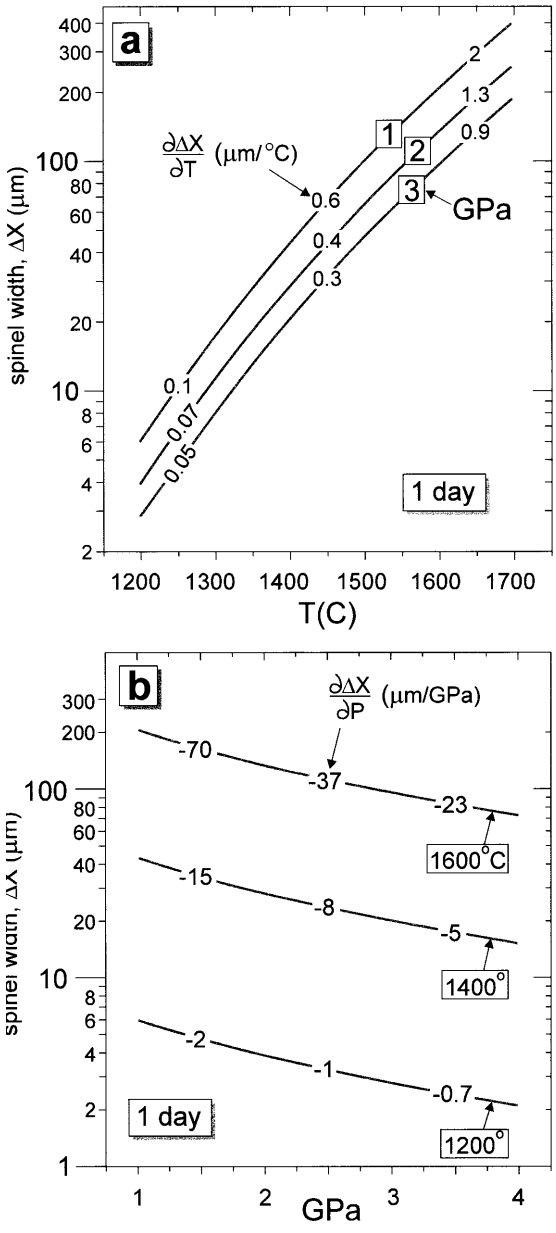


**Fig. 5a, b** Plots showing the temperature- and pressure-sensitivity of the reaction-progress thermo(bar)meter in terms of the thickness of spinel developed in a 1-day experiment at various conditions. In **a**, $\Delta X$ is shown as a function of temperature (°C) at 1, 2, and 3 GPa. In **b**, $\Delta X$ is plotted against pressure at three different temperatures. The values for the derivatives shown on the figures provide an indication of the magnitude of temperature or pressure differences that might be resolved, given that $\Delta X$ can be measured to within ~1–2 μm, depending on the nature of the materials and the measurement method used (see text)

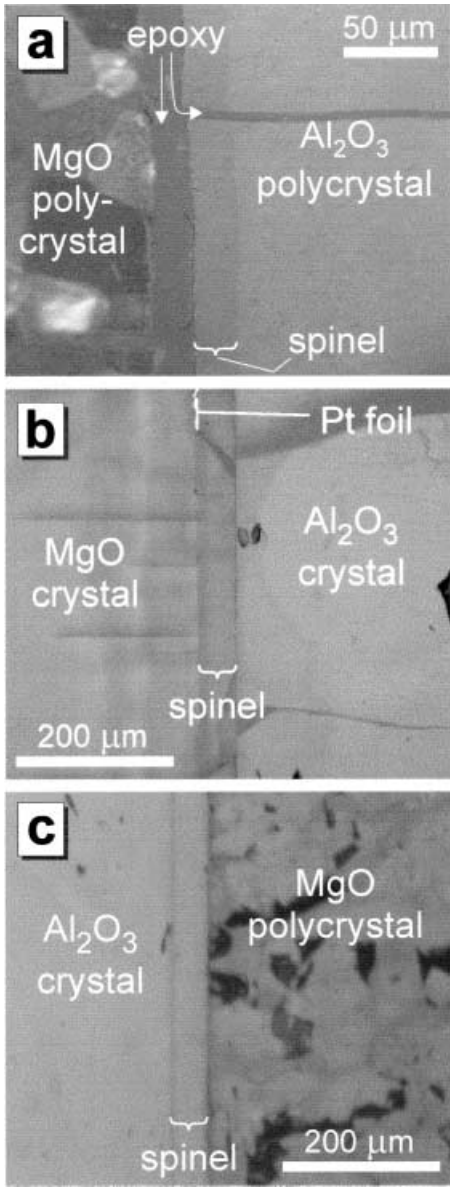


**Fig. 6a–c** Reflected-light photomicrographs of spinel layers and contacting MgO and $Al_2O_3$ in selected experiments. In **a**, both the MgO and the $Al_2O_3$ are polycrystalline, resulting in boundaries against spinel that are somewhat wavy (run 27). Photos **b** and **c** show a single crystal of corundum bounded initially on the left by a single crystal of periclase and on the right by polycrystalline MgO (run 48). In both cases, the resulting spinel layer has sharp, planar boundaries against the reacting phases. The Pt foil in **b** was intended to mark the original interface (see Watson and Price 2001). The cracks are decompression features

Fig. 7). Six axis-parallel temperature profiles are shown in the upper left panel of the figure, which collectively reveal that the hot zone is broader both axially and radially than in the standard assembly. The axial profile includes a hot zone ~12 mm long in which temperature varies by ~20°. Despite some apparent "fine-structure", the radial profile is relatively flat, as evidenced by the near-coincidence of the six axial profiles. The hot zone in this assembly appears in the contour plot as a broad plateau more-or-less bounded by the graphite insert. The axial profiles of runs 47 and 56 are compared directly in the lower left panel of Fig. 11. The effects of the stepped heater are qualitatively similar to the model predictions of Wunder and Schilling (1999).

The final test application of the spinel reaction-progress thermometer in the piston-cylinder was to use it in a "real" experiment to monitor the temperature

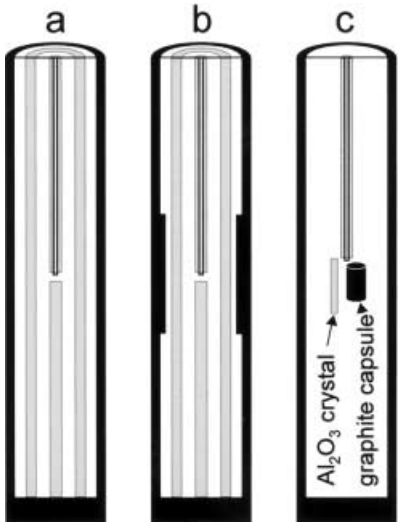


**Fig. 7a–c** Schematic sections of the internal filler-piece arrangements used to map temperature distribution in 19-mm diameter assemblies (legend as in Fig. 2). See text for discussion

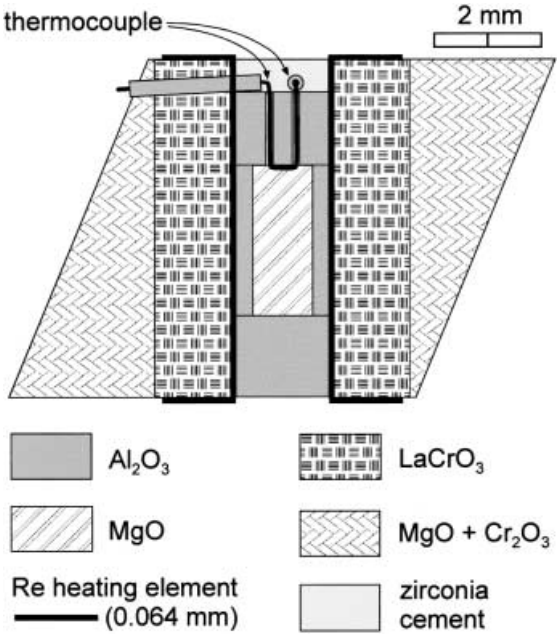


**Fig. 8** Schematic section of the octahedral assembly used for exploratory thermal mapping of multi-anvil experiments (run nos. MA1 and MA3; see Table 1 and text for discussion)

gradient in a graphite capsule. The capsule were positioned in a 19-mm assembly as shown in Fig. 7c, parallel to a small slab of single-crystal corundum. The objective of the experiment was to achieve microstructural equilibration of basaltic melt and olivine at 1.0 GPa and a reasonable upper mantle temperature of 1,275 °C. This is well below the temperature of the thermal mapping experiments described above, and approaches the lower end of the easily usable range of our thermometer. The results are shown in Fig. 12, which reveals a ~4-mm hot zone with a temperature spread of ~15°. The contained sample was much shorter than 4 mm, so the observed gradient was acceptable in terms of its possible effects on the phase equilibria (although it did cause difficulties with the microstructure because melt tends to migrate even in a small T gradient). The thermal profile shown in Fig. 12 is somewhat steeper than the one in run 47 (Fig. 10), probably because much of the filler material in the run 47 assembly was dense $Al_2O_3$, which has a higher thermal conductivity than MgO at high temperatures (Lide 1998). Despite the difficulties with sample microstructure, the experiment was unequivocally successful in showing that the spinel thermometer can be used as a routine temperature-gradient monitor at conditions relevant to melting in the upper mantle.

Thermal mapping results from the exploratory multi-anvil runs are shown in Fig. 13, which includes axial profiles for assemblies at 14 GPa and nominal temperatures of 1,700 and 1,975 °C (runs MA1 and MA3, respectively). A few aspects of the experiments and the figure differ from the preceding descriptions. It should be emphasized that, first, we have not actually calibrated the temperature dependence at 14 GPa: for the purpose of constructing the diagram, we assumed that the temperature dependence of spinel growth is the same at 14 GPa as at 1–4 GPa. It is important to note

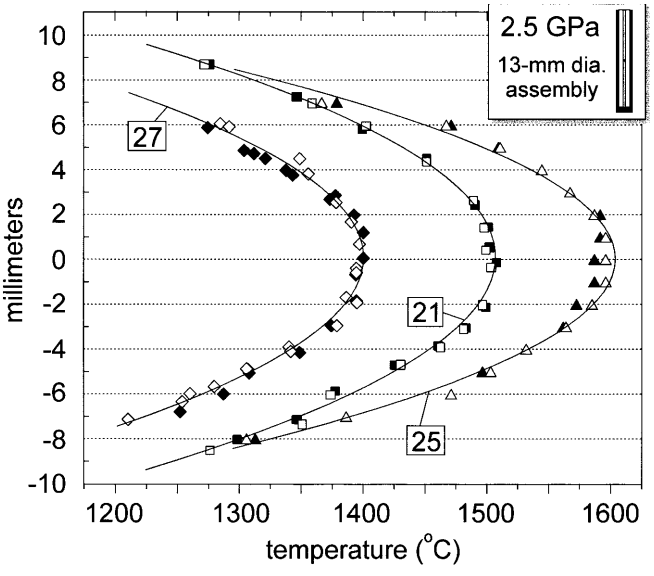


**Fig. 9** Axial thermal profiles of 13-mm diameter assemblies from runs 21, 25, and 27. The *open* and *filled symbols* represent temperatures recorded on opposite sides of the thermocouple insulator. The filler-piece configuration in all three runs was as in Fig. 2b (*see inset*). See text for discussion of the uncertainties in the individual temperature estimates and the significance of the parabolic fits (*smooth curves*)

that, also, the thermocouple was lost near the start of run MA3, and the experiment was continued for 2.3 h by maintaining constant power to the furnace. For this reason, the time-integrated temperature is not accurately known anywhere in the assembly. The temperatures shown were obtained by extrapolation

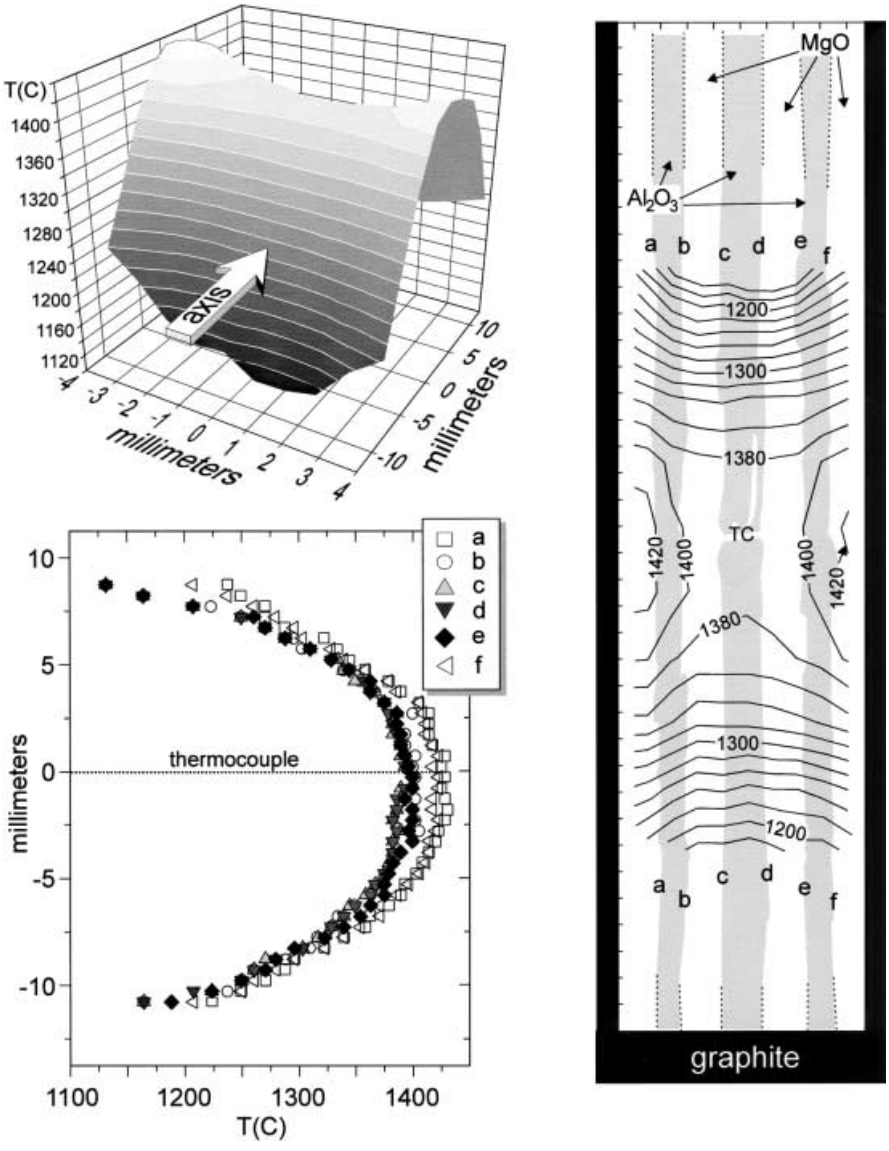


**Fig. 10** Thermal structure of "standard" 19-mm diameter assembly used in the RPI lab. Letters *a–f* on the contour map and 2-D graph refer to six axis-parallel lines of contact between polycrystalline MgO (*white*) and $Al_2O_3$ (*gray*) along which spinel thickness was measured at ~500-μm intervals. The irregularity in these contacts is caused by brittle deformation of the $Al_2O_3$ on pressurization. The *tick marks* along the graphite heater are spaced at 1 mm. See text for discussion

from the spinel thicknesses measured in the 14-GPa run at 1,700 °C (no. MA1) using the temperature dependence determined at lower pressures in the piston-cylinder (significantly, this extrapolation yields an estimated temperature for run MA3 that is consistent with that given by the known power vs. temperature curve for the multi-anvil device in which the experiments were run). Despite these limitations, the plotted temperature profile for run MA3 is believed to be a reasonable representation of relative changes in temperature along the assembly.

## Concluding remarks

The spinel reaction-progress thermometer should be useful to piston-cylinder practitioners involved in many types of investigations at temperatures exceeding ~1,200 °C. Its ease of use in thermal mapping applications makes the thermometer a valuable alternative and complement to numerical simulations of the thermal structure in piston-cylinder assemblies (see, e.g., Wunder and Schilling 1999). On the basis of our two exploratory experiments, it seems clear that implementation of our thermal mapping approach in multi-anvil devices is a realistic goal, despite the negative pressure dependence of the spinel growth rate [see Eq. (2) and Fig. 5]. Provided the conditions of interest lie within the stability field of spinel (i.e., so MgO and $Al_2O_3$ will actually react; see Akaogi et al. 1999), Eq. (2) appears to be useful as a rough indicator of spinel growth at multi-anvil pressures. A measurable spinel layer (i.e., on the order of 5 μm thick) will develop in ~1 day at the following conditions (GPa/T °C): 5/1,300, 10/1,400, 15/1,500 (spinel is not stable at $P > 17$ GPa at 2,000 °C; Akaogi et al. 1999). These hopeful predictions are broadly confirmed by our initial multi-anvil results, but it is also clear that quantitative multi-anvil applications must await a

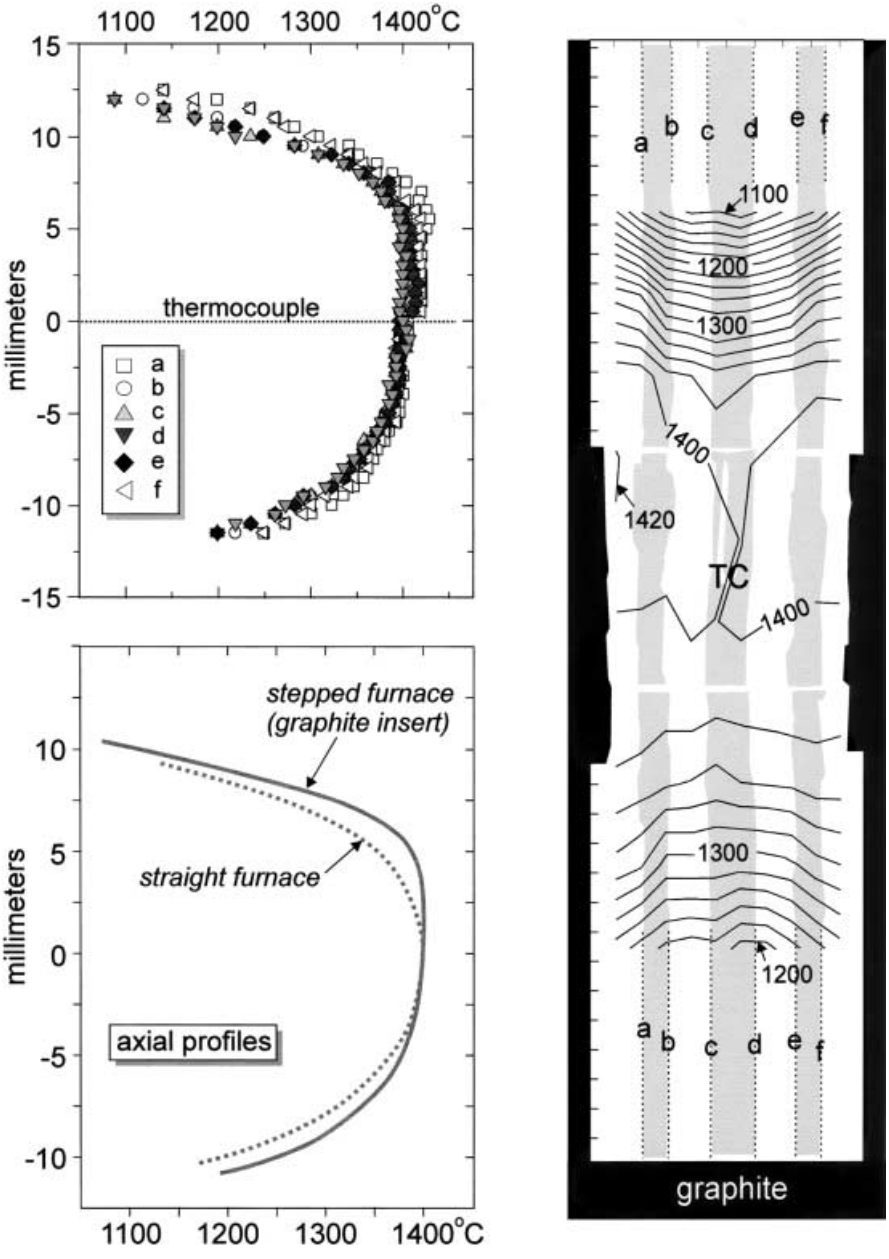


**Fig. 11** Thermal structure of 19-mm assembly fitted with a graphite insert to create a stepped heater (see Fig. 7b). The *insert* was initially 14 mm long with a ~0.5-mm wall thickness, but underwent appreciable compaction and deformation during pressurization. The axial thermal profiles of assemblies with stepped and straight heaters are compared in the *lower left panel* (see text)

thorough calibration at the relevant pressures. Watson and Price (2001) showed that rate of spinel growth depends critically on the solubility of $Al_2O_3$ in the spinel lattice, which is sensitive to both temperature and pressure. Interestingly, if future calibration experiments are conducted with single-crystal oxides, the results might be sufficiently accurate and precise to use the extent of spinel growth as an internal pressure monitor, or as a way of calibrating pressure in other devices.

Apart from exploring the thermal structure of new furnace designs in the RPI lab, we will use spinel growth at $MgO/Al_2O_3$ contacts primarily as a monitor of the temperature field surrounding our samples (as in Fig. 7c). However, spinel growth has already proved useful as a means of calculating the duration of experiments in which the thermocouple failed unexpectedly. In a similar vein, spinel thickness could be used as a recorder of time-integrated temperature of experiments controlled by power regulation rather than by a thermocouple (indeed, run MA3 of this study – in which the thermocouple failed at the start of the run – could have been salvaged for quantitative applications if the reaction-progress thermometer had been calibrated previously). We are also exploring the possibility of using spinel thickness to reconstruct the temperature of capsules strategically positioned at different vertical positions in a single piston-cylinder assembly. It may be advantageous under some circumstances to run polythermal series of experiments simultaneously.

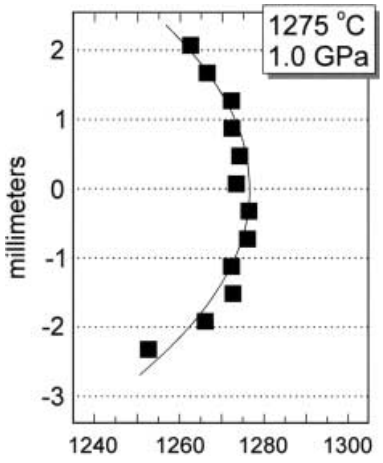


**Fig. 12** Axial temperature profile near the hot zone of a standard 19-mm diameter assembly containing a graphite capsule. In this case, the thermometry was done at the contact between single-crystal corundum and polycrystalline MgO (see text and Fig. 7c)

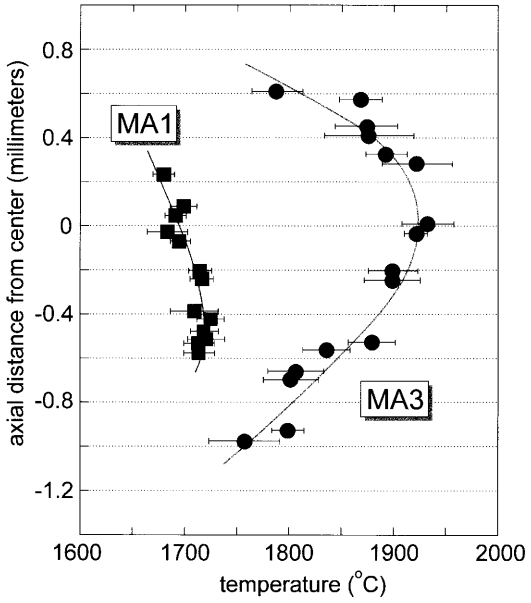


**Fig. 13** Partial axial temperature profiles of the sample regions of two multi-anvil assemblies. Note that the higher-temperature experiment (MA3) was completed by maintaining constant power to the furnace following loss of the thermocouple early in the run, so the absolute temperatures are not accurately known in this case. See text for discussion and Fig. 8 for assembly details

In summary, spinel reaction progress can be used to map the thermal structure of solid media assemblies with accuracy and spatial detail. This capability should reduce some of the uncertainties inherent in piston-cylinder and multi-anvil experimentation. We hope it will also stimulate innovation in experiment design that go beyond the routine applications discussed above.

**Acknowledgements** This work was conducted mainly to refine and improve the overall experimental capabilities and techniques used in the RPI high-pressure lab. In that respect it was supported by the two agencies that provide project-specific funds to the lab: the National Science Foundation (grant nos. EAR-9804794 and EAR-0073752) and the US Department of Energy (grant no. DE-FG02-94ER1443). J.A. has been supported by an NSF Postdoctoral Fellowship and the Carnegie Institution of Washington. All sources of support are gratefully acknowledged, as are the official reviews of David Walker and Steve Parman.

## References

Akaogi M, Hamada Y, Suzuki T, Kobayashi M, Okada M (1999) High pressure transitions in the system $MgAl_2O_4$–$CaAl_2O_4$: a new hexagonal aluminous phase with implication to the lower mantle. Phys Earth Planet Int 115:67–77

Bertka CM, Fei Y (1997) Mineralogy of the Martian interior up to core-mantle boundary pressures. J Geophys Res 102:5251–5264

Boyd FR, England JL (1960) Apparatus for phase equilibrium measurements at pressures up to 50 kb and temperatures up to 1,750 °C. J Geophys Res 65:741–748

Carter RE (1961) Mechanism of solid-state reaction between magnesium oxide and aluminum oxide and between magnesium oxide and ferric oxide. J Am Ceram Soc 44:116–120

Kushiro I (1976) Changes in viscosity and structure of melt of $NaAlSi_3O_8$ composition at high pressures. J Geophys Res 81:6347–6356

Lesher CE, Walker D (1986) Solution properties of silicate liquids from thermal diffusion experiments. Geochim Cosmochim Acta 50:1397–1411

Lesher CE, Walker D (1988) Cumulate maturation and melt migration in a temperature gradient. J Geophys Res 93:10295–10311

Li DX, Piroux P, Heuer AH, Yadavalli S, Flynn CP (1992) A high-resolution electron microscopy study of $MgO/Al_2O_3$ interfaces and $MgAl_2O_4$ spinel formation. Philos Mag A 65:403–425

Lide DR (1998) Handbook of chemistry and physics, 79th edn. CRC Press, Boca Raton

MacKenzie KJD, Ryan MJ (1981) Effect of electric fields on solid-state reactions between oxides. J Mater Sci 16:579–588

Mao HK, Bell PM (1971) Behavior of thermocouples in the single-stage piston-cylinder apparatus. Carnegie Inst Wash Yearbook 69:207–216

Rossi RC, Fulrath RM (1963) Epitaxial growth of spinel by reaction in the solid state. J Am Ceram Soc 46:145–149

Takahashi E (1986) Melting of dry peridotite KLB-1 up to 14 GPa: implications on the origin of peridotitic upper mantle. J Geophys Res 91:9367–9382

Tammann G (1920) Über Anlauffarben von Metallen. Z Anorg Allg Chem 111:78–99

Ting C-J, Lu H-Y (1999) Defect reactions and the controlling mechanism in the sintering of magnesium aluminate spinel. J Am Ceram Soc 82:841–848

Van Westrenen W, Van Orman JA, Fei Y, Watson EB (2001) Temperature distribution in multi-anvil assemblies derived from spinel layer growth. EOS Trans Am Geophys Union, Fall Meeting Abstracts

Walker D, Agee CB (1988) Ureilite compaction. Meteoritics 23:81–91

Walker D, Lesher CE, Hays JF (1981) Soret separation of lunar liquid. Proc Lunar Planet Sci 12B:991–999

Wark DA, Watson EB (2001) Grain-scale channelization of pores due to gradients in temperature or composition of intergranular melt. J Geophys Res (in press)

Watson EB, Price JD (2001) Kinetics of the reaction MgO + $Al_2O_3 \rightarrow MgAl_2O_4$ and Al–Mg interdiffusion in spinel at 1,200–2,000 °C and 1.0–4.0 GPa. Geochim Cosmochim Acta, (in press)

Watson EB, Wark DA (1997) Diffusion of dissolved $SiO_2$ in $H_2O$ at 1 GPa, with implications for mass transport in the crust and upper mantle. Contrib Mineral Petrol 130:66–80

Whitney WP II, Stubican VS (1971a) Interdiffusion studies in the system $MgO–Al_2O_3$. J Phys Chem Solids 32:305–312
Whitney WP II, Stubican VS (1971b) Interdiffusion in the system $MgO–MgAl_2O_4$. J Am Ceram Soc 54:349–352
Wunder B, Schilling FR (1999) Temperature distribution in piston cylinder cells: modelling and experiments. EOS Trans Am Geophys Union 80:F1116
Yamaguchi G, Tokuda T (1967) Some aspects of solid state reactions between oxides. Bull Chem Soc Jpn 40:843–851
Zhang P, DebRoy T, Seetharaman S (1996) Interdiffusion in the $MgO–Al_2O_3$ spinel with or without some dopants. Metall Mater Trans A 27A:2105–2114